INRIA

INSTITUT NATIONAL DE RECHERCHE EN INFORMATIQUE ET EN AUTOMATIQUE

Numerical Comparison of SVD and Propagator/Reflectivity Decomposition for the Acoustic Wave Equation

Valery Khajdukov , Victor Kostin , Vladimir Tcheverda , François Clément , Guy Chavent

N° 2888

Mai 1996

THÈME 4

ISSN 0249-6399

INRIA
ROCQUENCOURT

Numerical Comparison of SVD and Propagator/Reflectivity Decomposition for the Acoustic Wave Equation

Valery Khajdukov*, Victor Kostin**, Vladimir Tcheverda***, François Clément , Guy Chavent

Thème 4 — Simulation
et optimisation
de systèmes complexes
Projet Estime

Rapport de recherche n°2888 — Mai 1996 — 20 pages

Abstract: In acoustic seismic-reflection experiments, because of the lack of low frequencies in the usual seismic sources, the reflection of the energy back to the surface is associated to the short wavelengths of the slowness (the "reflectivity" parameters), while the long wavelengths of the slowness (the "propagator" parameters) are associated to the kinematics of the arrival times of this energy. Such a decomposition between the propagator and reflectivity parameters is automatic when a linearized model is used, but can only approximately be satisfied in the case of the full (non linearized) acoustic model.

In the 2D case, the embedded sequence of subspaces built by bilinear interpolation at the nodes of subgrids provides the slowness space with a hierarchical basis which allows a simple multiscale analysis and leads to the choice of two orthogonal subspaces for the propagator and reflectivity unknowns.

This paper is devoted to the mathematical justification of the previous propagator/reflectivity decomposition by means of singular value decomposition (SVD) analysis of the Frechet derivative of the modeling operator mapping the slowness to the surface data in the case of the 2D acoustic wave equation. It is shown numerically that the propagator/reflectivity decomposition is associated to a truncated SVD.

Key-words: acoustic wave equation, MBTT formulation, propagator/reflectivity decomposition, linearization, Frechet derivative, compact operator, singular value decomposition (SVD)

(Résumé : tsvp)

The research described in this publication was made as a part of the project "Numerical Methods to Solve Identification Problems in Geophysics" of l'Institut Franco-Russe A.M. Liapunov d'Informatique et de Mathématiques Appliquées and was partly supported by Russian Foundation of Basic Research Grant N 96-01-01515

* Institute of Geophysics, Siberian Division of Russian Academy of Sciences, Novosibirsk, 630090, Russia.
** Institute of Mathematics, same address.
*** Computing Center, same address.

Comparaison numérique de la décomposition en valeurs singulières et de la décomposition propagateur/réflectivité pour l'équation des ondes acoustiques

Résumé : Lors d'expériences de sismique-réflexion acoustique, en raison du faible contenu basse-fréquence des sources sismiques courantes, la réflexion de l'énergie vers la surface est associée aux courtes longueurs d'ondes de la lenteur (les paramètres "réflectivité"), alors que les grandes longueurs d'ondes de la lenteur (les paramètres "propagateur") sont associées à la cinématique des temps d'arrivées de cette énergie. Une telle décomposition entre les paramètres propagateur et réflectivité est automatique quand un modèle linéarisé est utilisé, mais peut seulement être satisfaite de façon approchée dans le cas du modèle acoustique complet (non linéarisé).

Dans le cas 2D, la suite emboîtée des sous-espaces construits par interpolation bilinéaire aux nœuds de sous-grilles pourvoit l'espace des lenteurs d'une base hiérarchique qui permet une analyse multiéchelle simple et mène au choix de deux sous-espaces orthogonaux pour les inconnues propagateur et réflectivité.

Cet article est dévolu à la justification mathématique de la décomposition propagateur/réflectivité précédente au moyen d'une analyse par décomposition en valeurs singulières de la dérivée de Frechet de l'opérateur de modélisation associant les données de surface à la lenteur dans le cas de l'équation des ondes acoustiques. Il est montré numériquement que la décomposition propagateur/réflectivité est associée à une décomposition en valeurs singulières tronquée.

Mots-clé : équation des ondes acoustiques, formulation MBTT, décomposition propagateur/réflectivité, linéarisation, dérivation de Fréchet, opérateur compact, décomposition en valeurs singulières

1 Introduction

The simplest mathematical model of the seismic wave propagation is initial-boundary value problem for a wave equation

$$n^2(x,z)\frac{\partial^2 u}{\partial t^2} = \Delta u + f(t)\delta(x-x_s, z-z_s); \tag{1}$$

$$u|_{t=0} = \frac{\partial u}{\partial t}|_{t=0} = 0; \tag{2}$$

$$\frac{\partial u}{\partial z}|_{z=0} = 0. \tag{3}$$

Regarding the source function $f(t)$ as known, the wave field on the free surface $z = 0$ (i.e. seismogram) is a result of an action of some non-linear operator B on the slowness $n(x,z)$:

$$B[n] = u|_{z=0} \equiv u_0(x, x_s, t). \tag{4}$$

Within the scope of this mathematical model the fundamental problem of reflection seismology is to recover $n(x,z)$ by resolving non-linear operator equation (4).

In the 80's, when the development of the power of computers made it clear that numerical solution of (1)–(3) for realistic models of wave propagation velocity would become a routine step, great expectations were connected with the least squares waveform inversion, when the slowness is searched for as a minimum point of the cost function

$$\Phi[n] = \|B[n] - u_0\|^2$$

by means of local gradient techniques. This approach was proposed as early as 1979 for 1-D problems ([3]) and 1982 for multidimensional problems ([4]). But it has turned out that for source function $f(t)$ with band-limited spectrum $\Phi[n]$ possesses many parasitic local minima and has a very narrow domain of attraction for the global minimum that becomes smaller when the dominant frequency of $f(t)$ increases (see for example [5] for 1-D problem and [1], [6] for 2-D problem).

One of the reasons why these local minima arise is "phase shift problem", that can be explained empirically as follows. As a rule interior structure of an earth is a sequence of layers, each with smooth variations of mechanical parameters (slowness for the model under consideration) and with rough change of these parameters under transition from a layer to layer. So, one can write the real slowness as the sum

$$n(x,z) = n_r(x,z) + n_s(x,z) \tag{5}$$

where

- n_r is called **reflectivity** and describes the rapid change of the slowness;
- n_s is called **propagator** and represents slow variations of n (often n_s is refered as a "background" in the geophysical literature).

In this decomposition n_r is responsible for the return of the energy radiated by a source to the surface and hence for the information content of seismic reflection data, while n_s assigns the arrival times of this energy. So, if n_s is poorly determined there arises a significant shift between the arrival times for real and synthetic data and any algorithm based on the local gradient technique will try to match together parts of the synthetic and data which differ by one or more cycle skip and will thus stop at some meaningless local minima.

Under routine data processing the reflectivity and the propagator are usually determined separately:

- for a given propagator depth-migration operators produce a good image of the reflectivity provided the correct propagator is used;
- the classical tools for the determination of the propagator fall roughly into the three classes:
  1. stacking velocity analysis;
  2. reflection tomography, which tries to determine the propagator by adjusting the arrival times of reflected waves;

3. migration velocity analysis.

In many cases a clever combination of these two techniques allows a good determination of the earth structure. So, it seems to be natural to apply the same idea to full waveform inversion and to recover the reflectivity and the propagator separately. There are various approaches for implementation of this idea in least squares technique: Multiple Migration Fitting (Chavent and Jacewitz [7]), Migration-Based Travel Time Formulation (Chavent and Clement [1]), Differential Semblance Optimization (Symes and Carrazone [8], Symes and Kern [9], Gockenbach, Symes and Tapia [10]), Paraxial Wave Equation and Remodeling (Bunks et al. [11]). The common in all these approaches is the decomposition of the slowness as (5) and an estimation of the reflectivity from the data for a given current value of the propagator before a cost function is built up. This leads to a modified cost function

$$\mathcal{M}\Phi[n_s] = \|\mathcal{M}B[n_s] - u_0\|^2$$

where $\mathcal{M}B[n_s] = B[n_s + \mathcal{ES}[n_s, u_0]]$ and $\mathcal{ES}$ is an operator that estimates distribution of the reflectivity by the data and a current value of the propagator. Numerical simulations presented in the mentioned above papers confirm expectations that modified objective function is amenable to minimization by local optimization technique.

When the acoustic wave equation is taken as the mathematical model the necessary item in implementation of this approach is decomposition of the model space $\mathcal{N}$ (slowness) as the orthogonal sum [1] of two subspaces – propagator $\mathcal{N}_s$ and reflectivity $\mathcal{N}_r$. The attempt to describe this procedure as quantitatively as possible is done in [2]. It is based on the following physically reasonable conditions which have to be satisfied by subspaces of the propagator and the reflectivity:

1. *low reflectivity content of* $\mathcal{N}_s$: the synthetic seismograms computed with $n_s \in \mathcal{N}_s$ contain no sizeable reflections beside the direct arrivals;
2. *sufficient kinematic content of* $\mathcal{N}_s$: replacing $n \in \mathcal{N}$ by its projection $n_s \in \mathcal{N}_s$ does not deteriorate too much the quality of the migrated images;
3. *low kinematic content of* $\mathcal{N}_r$: replacing of $n_s \in \mathcal{N}_s$ by $n_s + n_r$ for any $n_r \in \mathcal{N}_r$ changes as little as possible the traveltimes between distant enough points

and consists in a multiscale decomposition of model space $\mathcal{N}$ on a fine grid (the largest scales are taken as the spaces of propagators while their orthogonal complements as the spaces of reflectivities).

Let us come back now to the non-linear operator equation (4). One of the usual technique to solve non-linear equations numerically is modified Newton method sometimes cited as Newton-Kantorovich method too ([12]). It consists in iterative process that presumes on each step resolution of the linear operator equation

$$DB[n_0] < n_{k+1} - n_k >= u_0 - B[n_k] \equiv \phi(x, x_s, t) \tag{6}$$

where $DB[n_0]$ is Frechet derivative of forward map B taken at some point n_0 lying not very far from exact solution. It happens (see Section 3), that if n_0 is a depth dependent function then for the ideal multicoverage system ($(x, x_s) \in R^2$ and $0 \le t < \infty$) equation (6) can be reduced to a linear operator equation

$$\mathcal{A} < n_{k+1} - n_k >= \psi$$

with a compact operator $\mathcal{A}$. This operator possesses the discrete singular spectrum $\sigma_1 \ge \sigma_2 \ge \dots \sigma_n \cdots \ge 0$ with zero as the only accumulating point and right singular vectors $u_1, u_2, \dots$ corresponding to this spectrum. This allows to decompose the model space as

$$\mathcal{N} = \mathcal{N}_{rank} \oplus \mathcal{N}_{rank}^{\perp} \quad \text{where} \quad \mathcal{N}_{rank} = span\{u_1, \dots, u_{rank}\}.$$

The objectives of the present paper is to compare this decomposition for different values of parameter $rank$ with the propagator/reflectivity decomposition.

The paper is organized as follows. Section 2 sketchy repeats the propagator/reflectivity decomposition following [2]. Section 3 deals with a formal derivation of the linear operator equation arising in implementation of the modified Newton method for an ideal multicoverage system. Section 4 contains the results of numerical SVD of $\mathcal{A}$ for homogeneous and vertically-inhomogeneous background. The numerical comparison of projections of Synclay model ([2]) onto $\mathcal{N}_r$ and $\mathcal{N}_{rank}$ for different values of parameter $rank$ are presented in this section as well.

[1] We suppose that $\mathcal{N}$ is a functional space with usual L_2 inner product

2 Propagator/reflectivity decomposition of the model space

Let us suppose the depth section is covered by the fine rectangular grid used for the numerical simulation of the initial–boundary value problem for the acoustic wave equation (1)-(3). Then the model space $\mathcal{N}$ is supposed to be made of functions defined by bilinear interpolation from their values at the nodes of the grid and a natural choice for $\mathcal{N}_s$ is the space of functions defined also by the same bilinear interpolation but on a coarse subgrid. Now, in order to obtain $\mathcal{N}_r$ one has to take the orthogonal supplementary subspace of $\mathcal{N}_s$ in $\mathcal{N}$.

Let us describe now Synclay model. This model is simple but realistic and is composed of five non-horizontal homogeneous layers leaning on a synclinal fold. The shallow layer is made of water. The values of wave propagation velocity are successively with depth 1500 m/s, 1800 m/s, 2300 m/s, 3000 m/s and 4000 m/s. The fine grid size is $h = 5.2\,m$, so the model of 1 km $\times$ 1 km is discretized on a 192$\times$192 finite difference grid. The sources were depthed at the $z_s = 10\,m$ with Ricker impulse as source function

$$f(t) = (1 - 2\pi^2\nu_0^2 t) \exp(-\pi^2\nu_0^2 t^2)$$

and dominant frequency $\nu_0 = 35\,Hz$. The recording duration of 1 s is sampled over 1250 time steps.

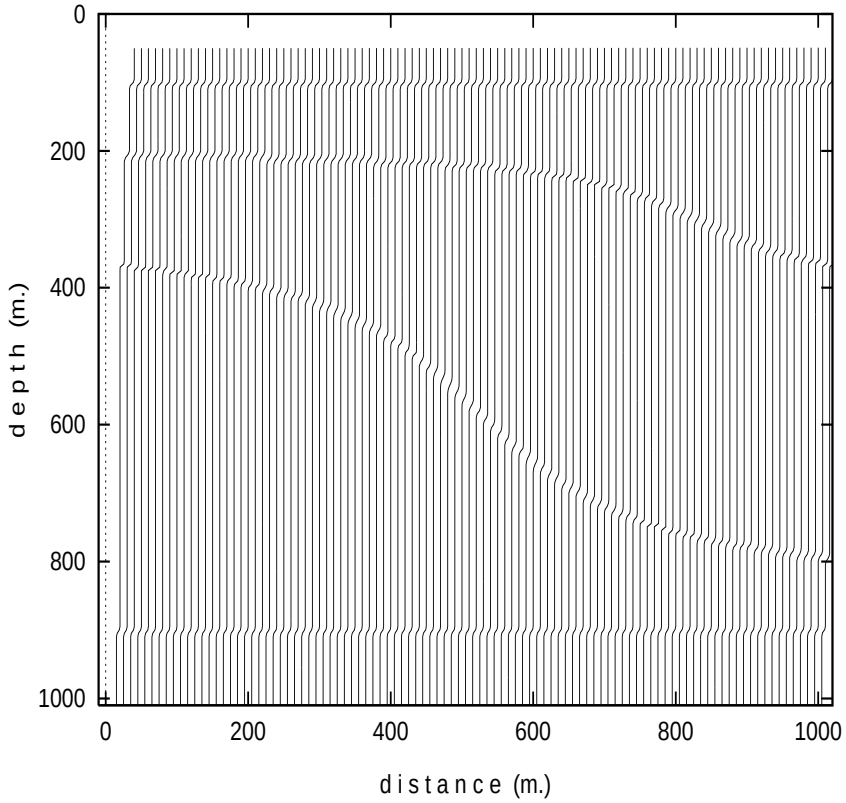

Figure 1: Synclay model (slowness)

In order to implement propagator/reflectivity decomposition Synclay model was initially discretized on the 192×192 mesh (fine grid) and then successively sampled by dichotomy to define seven scales of approximation ($192 = 3\times2^6$) from the coarsest grid 3×3 to the finest grid 192×192. At each scale M one can get decomposition

$$\mathcal{N}_M = \mathcal{N}_{M-1} \oplus \mathcal{W}_M$$

where $\mathcal{N}_M$ is the subspace that corresponds to the subgrid $3\cdot2^M \times 3\cdot2^M$ and $\mathcal{W}_M$ is the canonical complement to $\mathcal{N}_{M-1}$ in $\mathcal{N}_M$ (let us remind, that $\mathcal{N}_M$ is the space of bilinear functions with predetermined values at the nodes of the grid $3\cdot2^M \times 3\cdot2^M$). So, for any integer M_0 between 0 and 5 one has

$$\mathcal{N}_6 = \mathcal{N}_0 \oplus \mathcal{W}_1 \oplus \cdots \oplus \mathcal{W}_{M_0} \oplus \mathcal{W}_{M_0+1} \oplus \cdots \oplus \mathcal{W}_6$$

hence $\mathcal{N}_s = \mathcal{N}_0 \oplus \mathcal{W}_1 \oplus \cdots \oplus \mathcal{W}_{M_0}$ and $\mathcal{N}_r = \mathcal{N}_s^{\perp}$. Analyzing the quality of migrated images and intensity of reflections in synthetic data, the optimal values of M_0 were taken equal to 2 or 3 ([2]). The projection of the Synclay model onto reflectivity subspace for $M_0 = 2$ and $M_0 = 3$ are presented on Fig. 2 and Fig. 3.

For more detailed description of propagator/reflectivity decomposition the reader should be refered to [2].

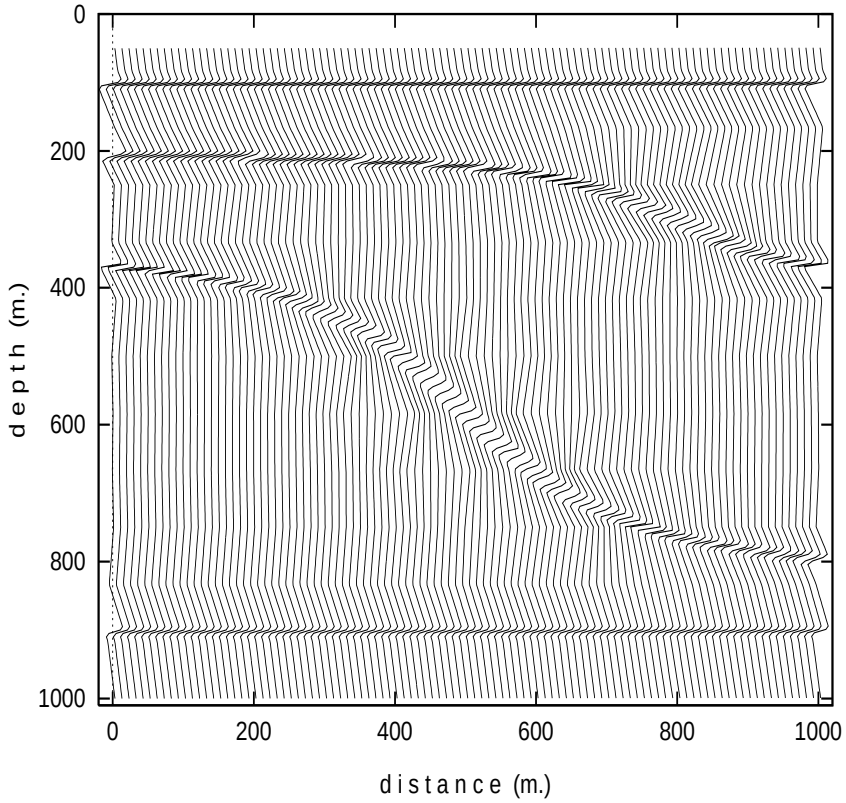

Figure 2: Reflectivity for Synclay model (M_0=2)

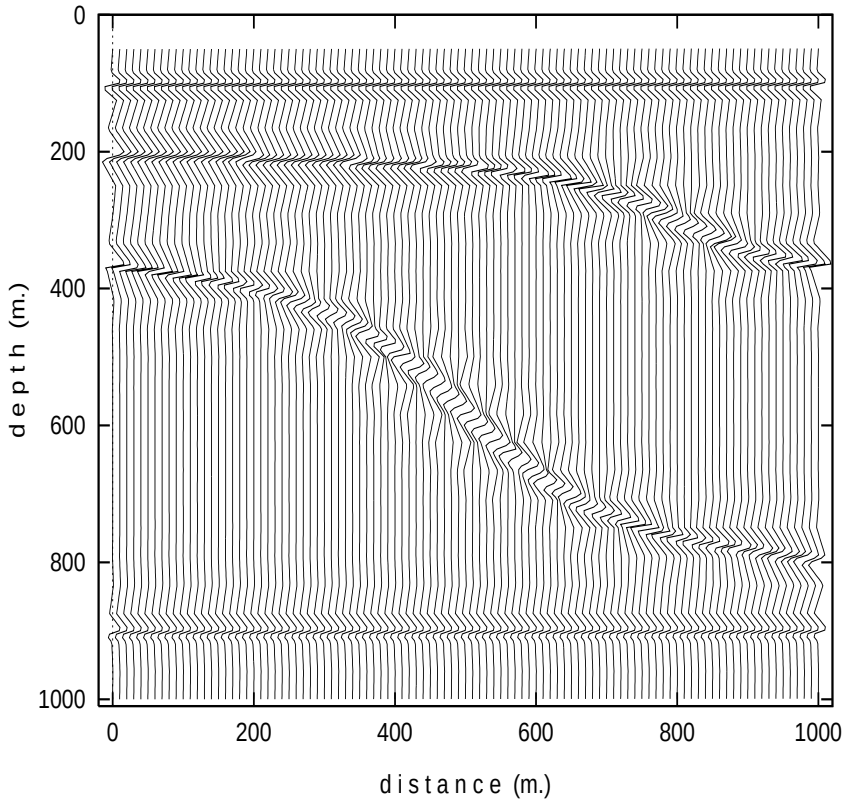

Figure 3: Reflectivity for Synclay model (M_0=3)

3 Formal analysis of the modified Newton method

Let us give at first some comments about differentiability of the operator B (forward map). When the spatial dimension is 1 or slowness depends only on vertical coordinate (layered problem) the properties of this operator have been studied fairly satisfactorily by Symes and others (see Symes [13] and [14] for references), while for multidimensional problems there are only partial results (Symes [15], [16], Sacks and Symes [17], Rakesh [18], Sun [19]). This is due to the fact that for the one dimensional wave equation both coordinate directions are spacelike, which indicates that the problem is hyperbolic with respect to both directions. Apparently, this is not the case when the spatial dimension is larger than one. Here we are not going to deal with the differentiability of B and concentrate instead on the studying of some properties of its formal derivative DB as the operator in Hilbert spaces (some suitable L_2 spaces).

In order to simplify considerations let us deal with the ideal multicoverage system, that is in (4) $(x, x_s) \in R^2$, $0 \le t < \infty$ and $L_2(R^2, R_+)$ is taken as the data space. The model space $\mathcal{N}$ is supposed to be consisted of the functions $n(x,z) = n_0(z) + n_1(x,z)$ with $\operatorname{supp} n_1(x,z) \subset [0,2a] \times [h,H]$ where $a > 0$, $h > z_s$, and $n_0(z) = n_\infty$ for $z \ge H - \varepsilon$, $\varepsilon > 0$. Next, let us assume that $n_1(x,z)$ on its support is represented as a trigonometrical sum of $2L+1$ summands

$$n_1(x,z) = \sqrt{\frac{1}{2a}} \sum_{l=-L}^{L} f_l(z) e^{i\frac{\pi l}{a}x} \tag{7}$$

with coefficients being L_2-functions on z on interval (h, H).

The formal linearization of the operator B at the point $n_0(z)$ presumes decomposition of the full wave field u as the sum $u_0 + u_1$ where u_0 is the wave field propagating within the reference medium while u_1 is scattered by the perturbation $n_1(x,z)$. The formal derivative DB is then a linear operator: $DB[n_0(z)] < n_1(x,z) >= u_1(x, 0; x_s; t)$ where $u_1(x, z; x_s; t)$ satisfies the initial-boundary value problem

$$\begin{aligned}
n_0^2(z)\frac{\partial^2 u_1}{\partial t^2} - \frac{\partial^2 u_1}{\partial x^2} - \frac{\partial^2 u_1}{\partial z^2} &= -2 \cdot n_1(x,z) n_0(z) \frac{\partial^2 u_0}{\partial t^2} \\
u_1|_{t=0} = \frac{\partial u_1}{\partial t}|_{t=0} &= 0 \\
\frac{\partial u_1}{\partial z}|_{z=0} &= 0 \\
n_0^2(z)\frac{\partial^2 u_0}{\partial t^2} - \frac{\partial^2 u_0}{\partial x^2} - \frac{\partial^2 u_0}{\partial z^2} &= f(t)\delta(x - x_s, z - z_s) \\
u_0|_{t=0} = \frac{\partial u_0}{\partial t}|_{t=0} &= 0 \\
\frac{\partial u_0}{\partial z}|_{z=0} &= 0
\end{aligned}$$

Let us now introduce function

$$U_1(z; k_x; k_s; \omega) = \lim_{\varepsilon \to 0} \int_0^\infty e^{i(\omega + i\varepsilon)t} dt \int_{-\infty}^{\infty} e^{ik_x x} dx \int_{-\infty}^{\infty} e^{ik_s x_s} u_1(x, z; x_s, z_s; t) dx_s$$

Under constraints $|k_x|$, $|k_s| < \omega n_{min}$ (n_{min} is the minimal value of $n_0(z)$) this function satisfies the boundary value problem ([20], Chap. 12 and [21], Chap. II)

$$\begin{aligned}
\frac{d^2 U_1}{dz^2} + (\omega^2 n_0^2(z) - k_x^2) U_1 &= -2 \cdot \omega^2 F(\omega) \hat{n}_1(k_x + k_s; z) n_0(z) G(z; z_s; k_s; \omega) \\
\frac{dU_1}{dz}|_{z=0} &= 0, \\
U_1|_{z>H} &= S(k_x; k_s; \omega) \exp\{iz\sqrt{\omega^2 n_\infty^2 - k_x^2}\}
\end{aligned}$$

where $S(k_x; k_s; \omega)$ is the amplitude of the outgoing wave, $\hat{n}_1(k; z)$ – Fourier transformation of $n_1(x,z)$ with respect to x, $F(\omega)$ – the spectrum of the source impulse $f(t)$ and $G(z; \zeta; k_s; \omega)$ – the Green function of the differential operator $\frac{d^2}{dz^2} + \omega^2 n_0^2(z) - k_s^2$ with the boundary conditions

$$\frac{dG}{dz}|_{z=0} = 0,$$

$$G|_{z>H} = V(k_x; k_s; \omega) \exp\{iz\sqrt{\omega^2 n_\infty^2 - k_x^2}\}.$$

In terms of this function each step of the modified Newton method converts to the recovering of functions $f_l(z)$ by the data

$$U_1|_{z=0} = \psi_{l,m}(\omega) \equiv \lim_{\varepsilon \to +0} \int_0^\infty e^{i(\omega + i\varepsilon)t} dt \int_{-\infty}^\infty e^{i\frac{\pi m}{a}x} dx \int_{-\infty}^\infty e^{i\frac{\pi(l-m)}{a}x_s} \phi(x, x_s; t) dx_s,$$
$$\frac{\pi|m|}{a},\ \frac{\pi|l-m|}{a} < \omega n_{min}, \quad \omega_1 \le \omega \le \omega_2$$

and consists in the resolution of the Fredholm integral equation of the first kind

$$A_{l,m} < f_l > \equiv$$
$$-\omega^2 F(\omega)\sqrt{2a} \int_h^H f_l(\zeta) n_0(\zeta) G(\zeta; z_s; \frac{\pi m}{a}; \omega) G(0; \zeta; \frac{\pi(l-m)}{a}; \omega) d\zeta = \psi_{l,m}(\omega); \tag{8}$$
$$|m|,\ |l-m| < \frac{a\omega n_{min}}{\pi}.$$

As $h > z_s \ge 0$, the kernel of integral operator $A_{l,m}$ is a bounded function and, so, it is the compact operator mapping $L_2(h, H)$ to $L_2(\omega_1^*, \omega_2)$ with

$$\omega_1^* = \max\left(\omega_1, \frac{|m|\pi}{a n_{min}}, \frac{|l-m|\pi}{a n_{min}}\right).$$

Because of the conditions on $|m|$ and $|l-m|$ in (8) f_l for $L > 2a\pi^{-1}\omega_2 n_{min}$ can not be found from these equations. So, below we will take $L \le 2a\pi^{-1}\omega_2 n_{min}$.

In order to treat system (8) as an operator equation with an operator defined on model space $\mathcal{N}$ let us introduce composite operator $\mathcal{A}_l$ and vector function ψ_l as

$$\mathcal{A}_l = \begin{pmatrix} A_{l,m_1} \\ A_{l,m_1+1} \\ \cdots \\ A_{l,m_2} \end{pmatrix}, \quad \psi_l = \begin{pmatrix} \psi_{l,m_1} \\ \psi_{l,m_1+1} \\ \cdots \\ \psi_{l,m_2} \end{pmatrix} \tag{9}$$

where second index m varies between m_1 and m_2 according to inequalities given in (8). Then (8) takes the form

$$\mathcal{A} < n_1 > = \begin{pmatrix} \mathcal{A}_{-L} & & & & & \\ & \mathcal{A}_{-L+1} & & & & \\ & & \ddots & & & \\ & & & \mathcal{A}_0 & & \\ & & & & \ddots & \\ & & & & & \mathcal{A}_L \end{pmatrix} \begin{pmatrix} f_{-L} \\ f_{-L+1} \\ \cdots \\ f_0 \\ \cdots \\ f_L \end{pmatrix} = \begin{pmatrix} \psi_{-L} \\ \psi_{-L+1} \\ \cdots \\ \psi_0 \\ \cdots \\ \psi_L \end{pmatrix} = \Psi \tag{10}$$

where $\mathcal{A}$ is the compact operator from $\mathcal{N}$ onto the space of vector functions defined on (ω_1, ω_2) with vector L_2 norm. The right singular vectors of this operator are $u_j^{(l)} exp(\frac{i\pi l}{a}x)$, where $u_j^{(l)}$ are right singular vectors of operator $\mathcal{A}_l$ corresponding to its singular values $\sigma_j^{(l)}$ being the singular values of $\mathcal{A}$ too. These right singular vectors form an orthogonal basis of the model space and we shall suppose that they are indexed in the order of decreasing singular values. So, we introduce orthogonal decomposition of this space as $\mathcal{N} = \mathcal{N}_{rank} \oplus \mathcal{N}_{rank}^\perp$ with $\mathcal{N}_{rank}$ being the linear span of the right singular vectors corresponding to singular values $\sigma_1, \sigma_2, \ldots, \sigma_{rank}$ where $rank$ is chosen such that $\sigma_{rank} > \sigma_{rank+1}$. This decomposition leads to a notion of r-solution ($r = rank$) of the linear operator equation of the first kind with a compact operator ([24]) generalized recently for a non-linear equation too ([25]). The natural features of r-solution is its stability and capacity to keep up the main peculiarities of a medium structure, particularly, its reflectivity distribution for not too large values of parameter $rank$ ([26]).

Remark 1 *Operators $\mathcal{A}^*$ and DB^* perform $(\omega - k)$ and space-time migration of residuals respectively ([22], [23]). This follows that $\mathcal{A}^*\mathcal{A}$ and DB^*DB should be rather close one to each other, i.e. their right singular vectors, being right singular vectors of $\mathcal{A}$ and DB as well, should be rather close too.*

A reason to expect that any propagator should be in $\mathcal{N}_{rank}^{\perp}$ for not too large values of $rank$ is the following. Let us suppose that background $n_0(z)$ belongs to the space of propagators. Then, in accordance with *low reflectivity contents of* $\mathcal{N}_s$ surface data $B[n_0] \approx 0$ and if $n_1(x,z)$ is a propagator too $B[n_0+n_1] \approx 0$. That follows $DB[n_0] < n_1 > \approx 0$ and, next, $\mathcal{A} < n_1 > \approx 0$. As right singular vectors of the operator $\mathcal{A}$ form the orthogonal base in the model space any function $n_1(x,z) \in \mathcal{N}$ can be represented as the sum

$$n_1 = \sum_{j=0}^{\infty} \sum_{l=-L}^{L} c_j^{(l)} u_j^{(l)} exp(i\frac{\pi l}{a}x)$$

So, if n_1 is from the space of propagators

$$\|\mathcal{A} < n_1 > \|^2 = \sum_{j=1}^{\infty} \sum_{l=-L}^{L} {\lambda_j^{(l)}}^2 {c_j^{(l)}}^2 \approx 0,$$

but that means that coefficients $c_j^{(l)}$ corresponding to rather large singular values $\sigma_j^{(l)}$ should be very small, that is n_1 should be "almost" orthogonal to $\mathcal{N}_{rank}$ for rather small values of $rank$. As both propagator/reflectivity decomposition and SVD are the orthogonal ones, subspace of reflectivity should be "almost" coincident with $\mathcal{N}_{rank}$.

4 Numerical SVD

Numerical SVD for compact operators $\mathcal{A}_l$ was implemented for two models of background: homogeneous with Synclay's mean value of velocity $c_0 = 2500$ m/s and linear ramp in depth from 1500 m/s (top) up to 4000 m/s (bottom). All considerations were performed within the square $0 \le x \le 1000\,m, \quad 50\,m \le z \le 1050\,m$, i.e. parameters a, h, H (see section 3) are 500 m, 50 m and 1050 m respectively. The model space $\mathcal{N}$ is supposed to be formed from functions representing as (7) with $L = 50$. In order to get finite dimensional approximation of linear operators $\mathcal{A}_l$ (i.e. its matrix representation) functions $f_l(z)$ in (8) were taken as piece-wise constant functions with step $\Delta z = 5$ m. In order to discretize the integral (8) with respect to ω 256 uniformly distributed dots were taken over interval $[0, 2\pi \cdot 100]$. So, for each l operator $\mathcal{A}_l$ is approximated by rectangular matrix $A_l^{(n)}$ with 200 columns and $(m2 - m1 + 1) \cdot 256$ rows. The background $n_0(z)$ was treated as a piece-wise constant function too. This allows to represent Green function $G(z; z_s; k; \omega)$ in the kernels of the operators A_l as

$$G(z; z_s; k; \omega) = C_1 \exp\{-i\lambda_1 z\} + D_1 \exp\{i\lambda_1 z\} + \exp\{i\lambda_1 |z - z_s|\}$$

within the first layer,

$$G(z; z_s; k; \omega) = C_j \exp\{-i\lambda_j z\} + D_j \exp\{i\lambda_j z\}$$

within all other layers,

$$G(z; z_s; k; \omega) = C_N \exp\{-i\lambda_N z\}$$

within the homogeneous half plane, where $\lambda_j = \sqrt{\omega^2 n_j^2 - k^2}$. Coefficients C_j, D_j are determined from the conditions

$$\frac{dG}{dz}|_{z=0} = 0$$

$$[G]\,|_{z=z_j} = \left[\frac{dG}{dz}\right]|_{z=z_j} = 0.$$

Numerical SVD was performed by means of LAPACK version 1.1. On Fig. 4 (homogeneous background) and Fig. 5 (linear ramp as background) common logarithms of singular values of matrices $\mathcal{A}_l$ are plotted as 51 graphs representing their dependence on index varying from 1 up to 200^2. The interesting peculiarity of these singular values, not obvious on their graphical representation, is that $\sigma_j^{(l)}$ decrease monotonically with respect to l under j fixed.

We illustrate the right singular vectors of matrix $\mathcal{A}_l^{(n)}$ for $l = 0$ on Fig. 6 (homogeneous background) and Fig. 7 (linear ramp as background). There are only 130 vectors because others correspond to very small singular values and are rather noisy. It is necessary to note, that singular vectors are extremely unsimilar for different

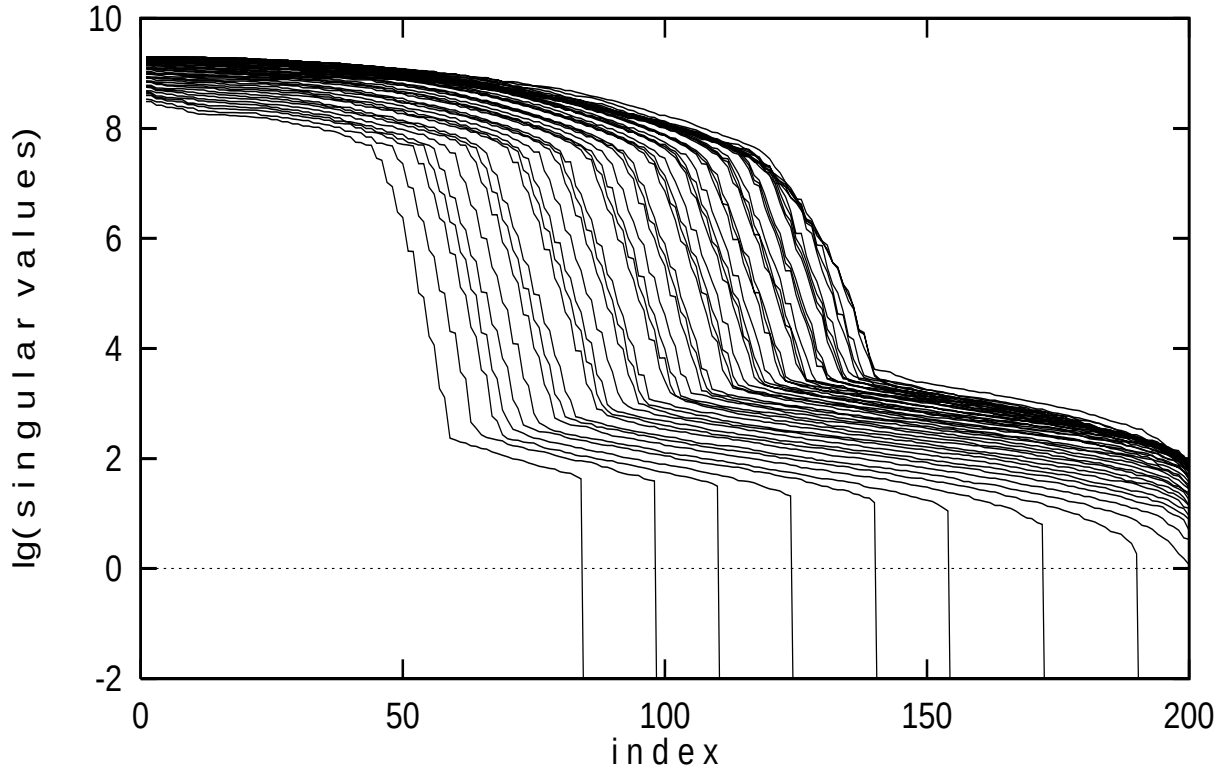

Figure 4: Singular values for homogeneous background

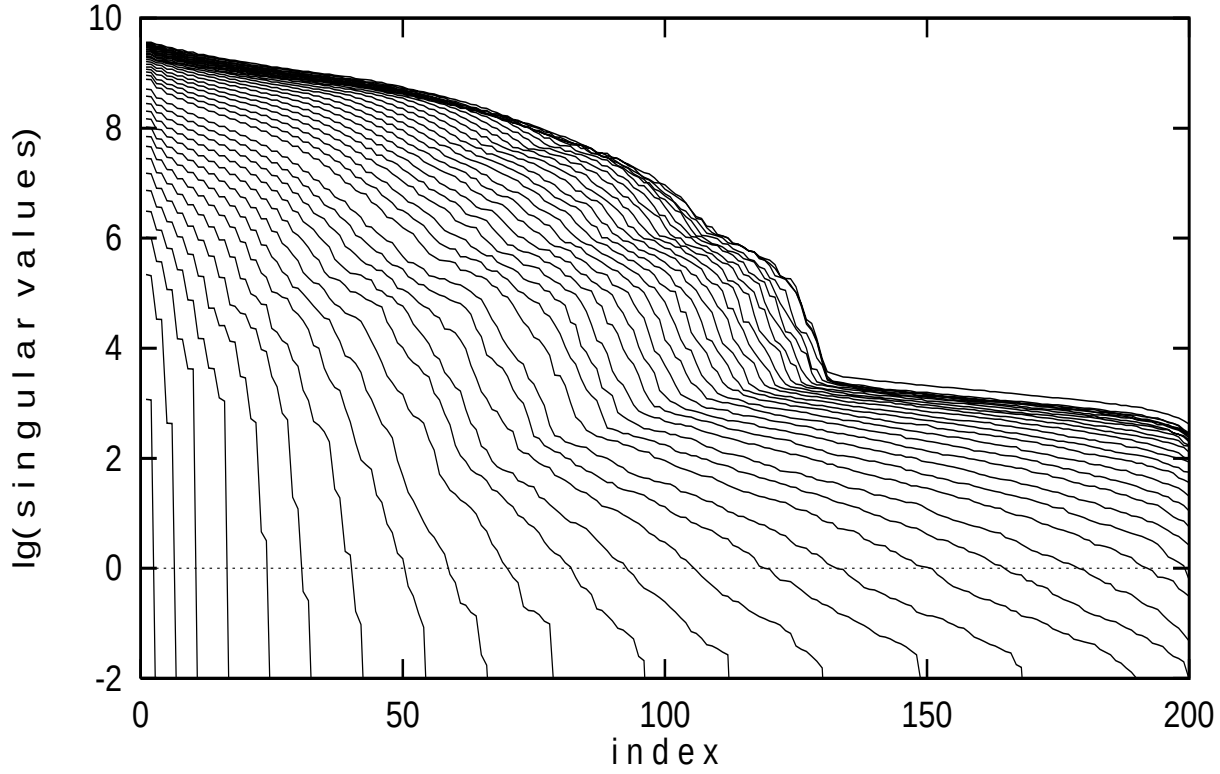

Figure 5: Singular values for linear ramp

a)

b)

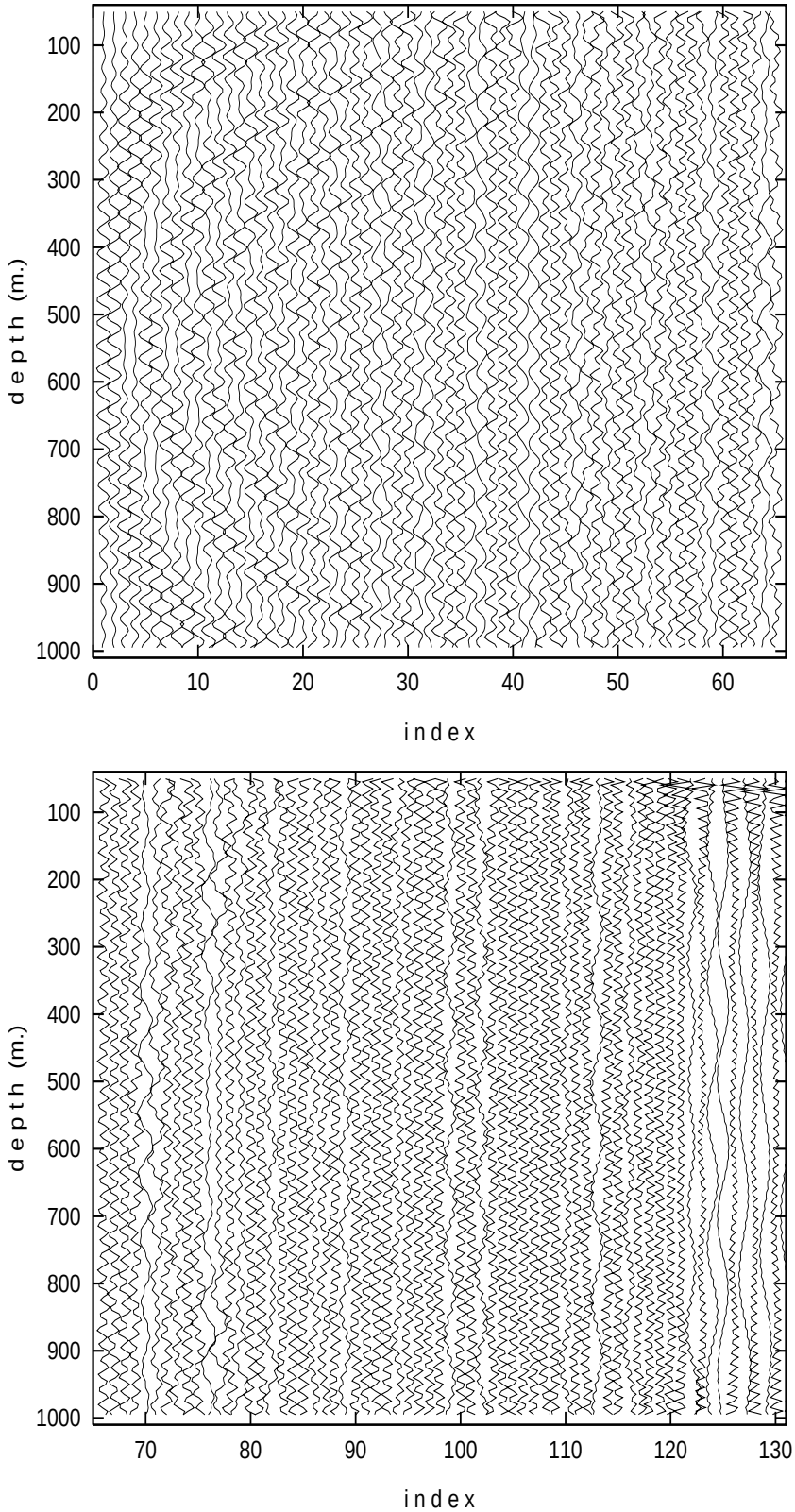

Figure 6: Right singular vectors for homogeneous background

a)

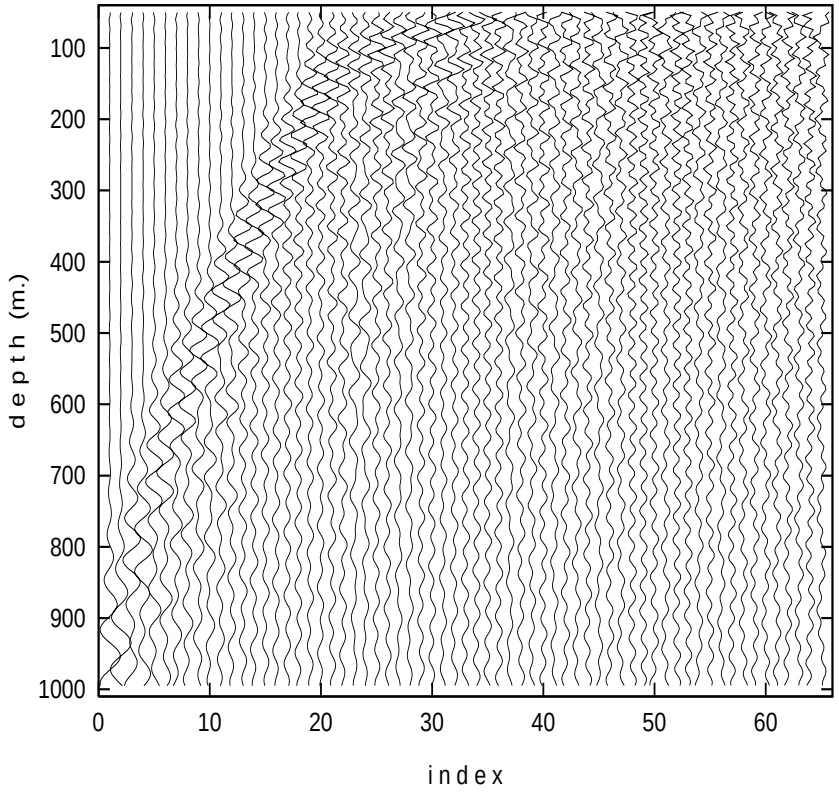

b)

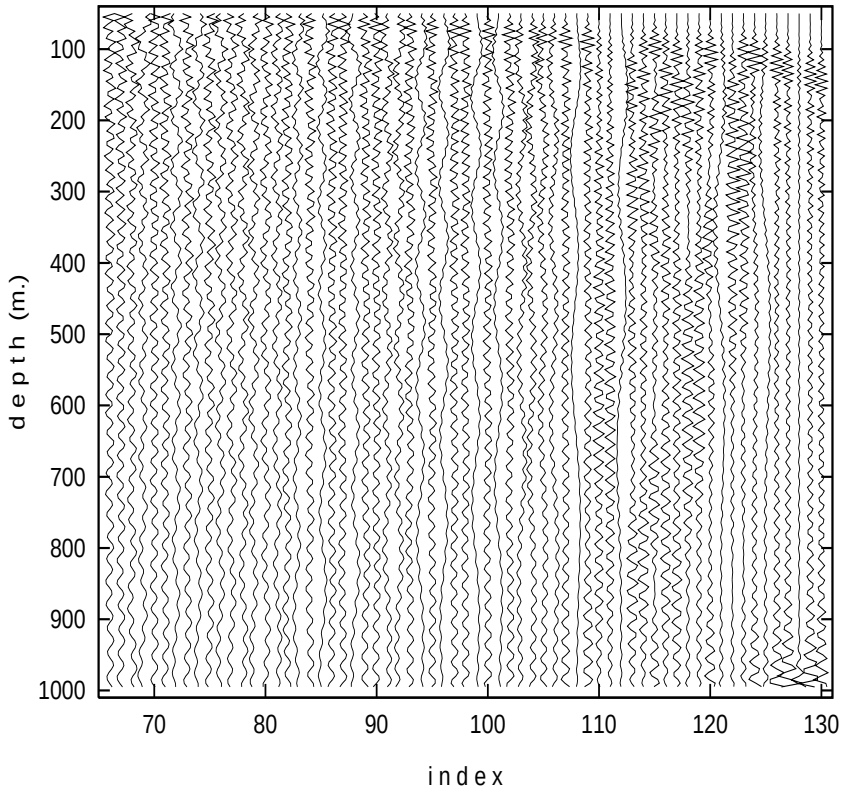

Figure 7: Right singular vectors for linear ramp

backgrounds, but their common feature is correspondence of slow oscillating ones (i.e. responsible for correction of propagator in iteration process (6)) to the rather small singular values.

In order to explain this feature let us consider the mutual disposition of Fourier base

$$\phi_m^{(n)}(x,z) = \frac{1}{\sqrt{2a(H-h)}} exp\{i\frac{\pi n}{a}x\} exp\{2i\frac{\pi m}{H-h}z\}.$$

with subspace

$$\mathcal{N}^{(\mu)} = span\left\{ u_k^{(l)} exp\{i\frac{\pi l}{a}x\};\, k,l:\ \frac{max\sigma_k^{(l)}}{min\sigma_k^{(l)}} \le \mu \right\} \tag{11}$$

This disposition can be specified by the angles $\alpha_m^{(n)}$ between $\phi_m^{(n)}$ and $U^{(\mu)}$ by computing for every m, l ($\phi_m^{(n)}$ and $u_k^{(l)} exp\{i\frac{\pi l}{a}x\}$ are orthogonal for $n \neq l$)

$$\cos\alpha_m^{(l)} = \|P^{(\mu)}\phi_m^{(n)}\| = \left(\sum_{k:\mu_k^{(l)} \le \mu} \left(\int_h^H exp\{2i\frac{\pi m}{H-h}z\} u_k^{(l)}(z)dz \right)^2 \right)^{\frac{1}{2}}$$

where $P^{(\mu)} : \mathcal{N} \longrightarrow \mathcal{N}^{(\mu)}$ is orthogonal projector onto linear subspace $\mathcal{N}^{(\mu)}$.

Remark 2 *As one can see $\mathcal{N}^{(\mu)} = \mathcal{N}_{rank}$ with $\mu = \sigma_1/\sigma_{rank}$ for indexed in the order of decreasing singular values σ_j. It should be noted here that μ is the condition number of the finite dimensional linear operator equation (projection equation for (10)):*

$$Q^{(\mu)}\mathcal{A}P^{(\mu)}n_1 = Q^{(\mu)}\psi \tag{12}$$

with $Q^{(\mu)}$ being a orthogonal projector onto subspace spanned left singular vectors of $\mathcal{A}$.

These cosines are plotted by three graphs ($l = 0,\ 25,\ 50$ from bottom to top respectively) in dependencies on index m for homogeneous background and linear ramp background for different values of parameter μ on Fig. 8–Fig. 9[3]. One can see that functions from Fourier base with low spatial frequencies with respect to depth z (for homogeneous background $m \le 20$ for $\mu \le 1.5$ and $m \le 10$ for $\mu \le 3.5$) are "almost" orthogonal to subspaces $\mathcal{N}^{(\mu)}$. This result one can take as an explanation of poor propagator recovering. The fact that $\mathcal{N}^{(\mu)}$ is "almost" orthogonal with respect to highly oscillating in space functions $\phi_m^{(l)}(x,z)$ (i.e. l and m are rather large) is connected with the well known Rayleigh criteria of resolving ability.

The last series of numerical experiments consists in computations of projections $P^{(\mu)}(n - n_0)$ for n being the slowness of Synclay model and n_0 - homogeneous and linear ramp background. They are represented on Fig. 10–Fig. 11.

One can see that projections corresponding to homogeneous background are much more noisy in comparison with ones for linear ramp. Apparently, this noise can be explained by the lack of slow variating with respect to depth functions in $\mathcal{N}^{(\mu)}$ and is not so much for linear ramp thanks to the less value of difference $n_1(x,z) = n(x,z) - n_0(z)$ along depth section (significant part of the propagator is already taken into account through linear ramp $n_0(z)$).

5 Discussion

Comparing decompositions of the model space produced by the different values of parameter *rank* in SVD of operator $\mathcal{A}$ and by the choice of "cursor position" in the propagator/reflectivity decomposition one can see that both of them produce "significant" and "non-significant" subspaces. For SVD a significant subspace is defined as a linear span of right singular vectors corresponding to the largest singular values, or, shortly speaking, a span of "largest right singular vectors", while for the approach based on the propagator/reflectivity decomposition such subspace is introduced as subspace of reflectivities. Non-significant subspaces should be defined as orthogonal complements to corresponding subspaces and for SVD it will be a span of "smallest" right singular vectors while

[2]The horizontal shelves for $lg\sigma_j \approx 3$ are presumed by finite computer accuracy and do not describe real distribution of singular values.

[3]These values of μ are predetermined by the choice of a number of right singular vectors $u_k^{(0)}$ of operator $\mathcal{A}_0$ taken in consideration. For both homogeneous background and linear ramp this number was taken equal to 35 ($\mu \le 1.5$ and $\mu \le 4$) and 75 ($\mu \le 3.5$ and $\mu \le 35$)

a)

b)

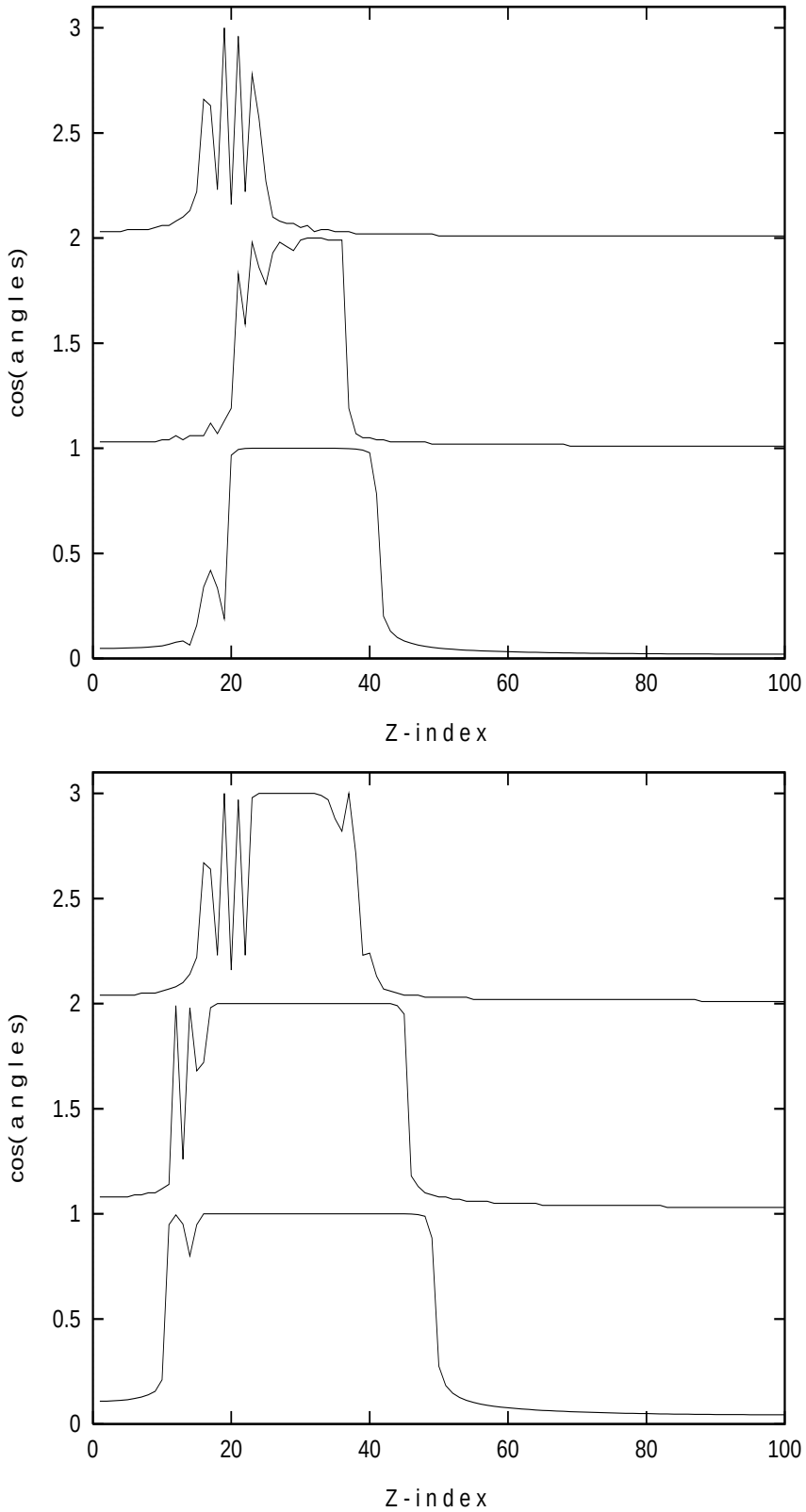

Figure 8: $\cos\alpha_m^{(l)}$ for homogeneous background: a) $\mu \leq 1.5$; b) $\mu \leq 3.5$

a)

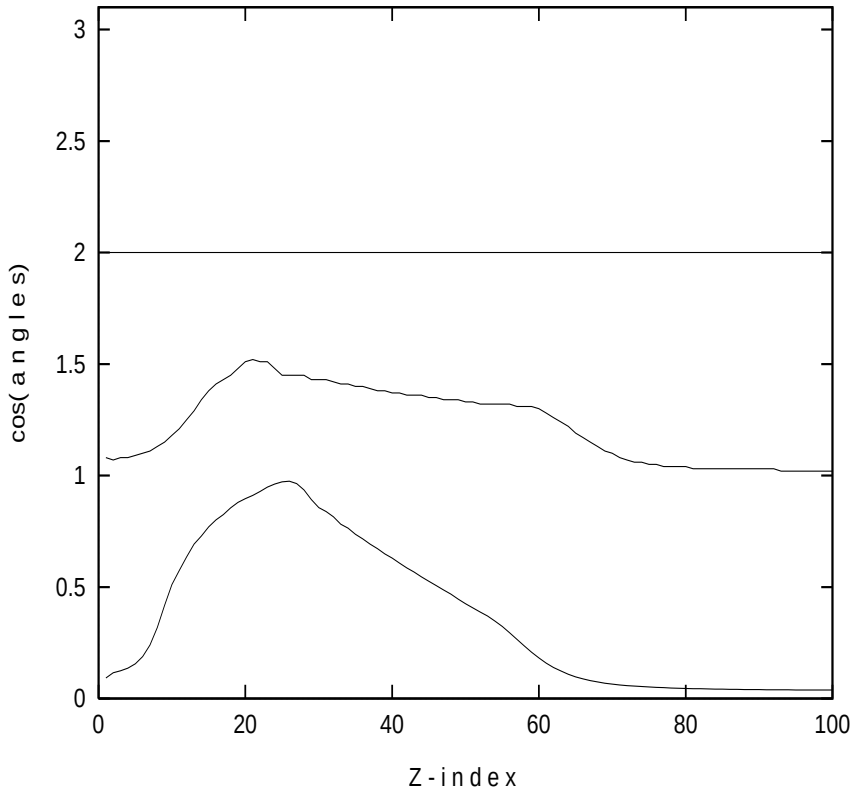

b)

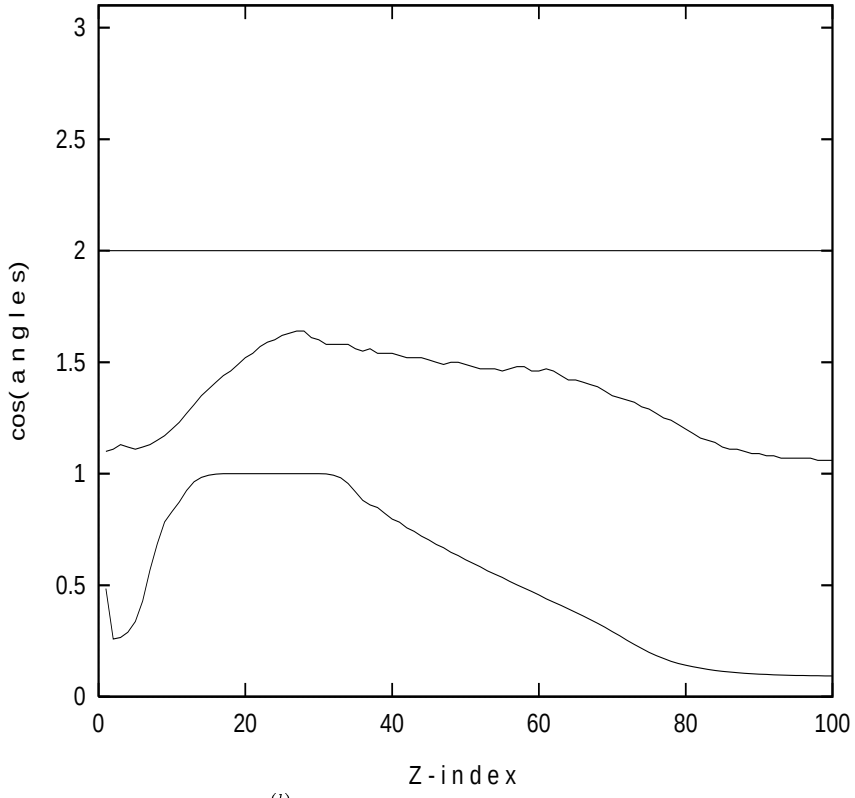

Figure 9: $\cos\alpha_m^{(l)}$ for linear ramp: a) $\mu \leq 2.5$; b) $\mu \leq 25$

a)

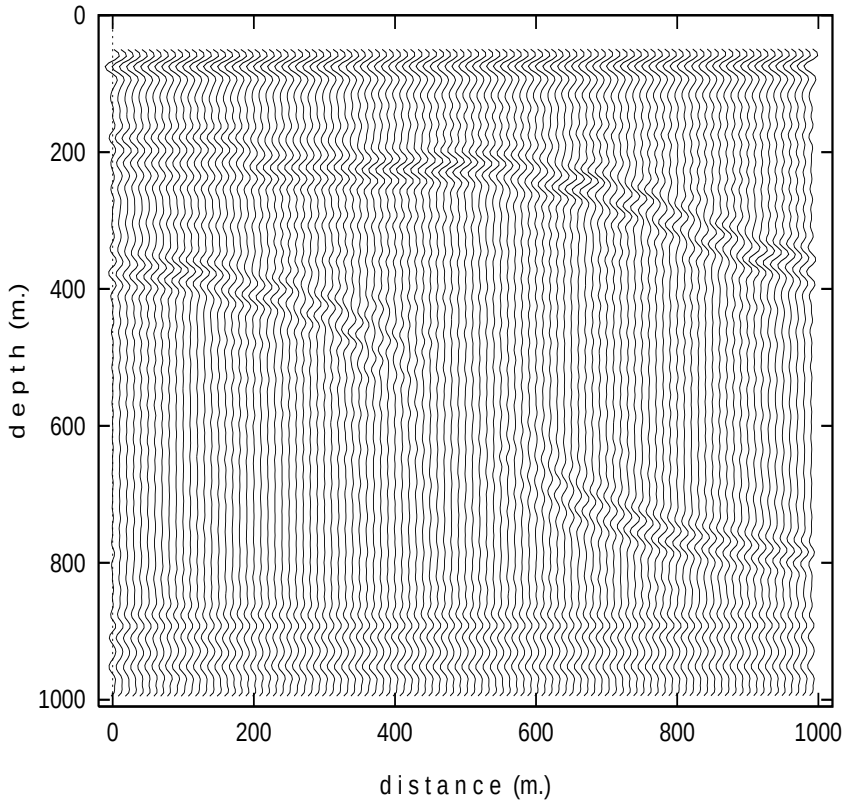

b)

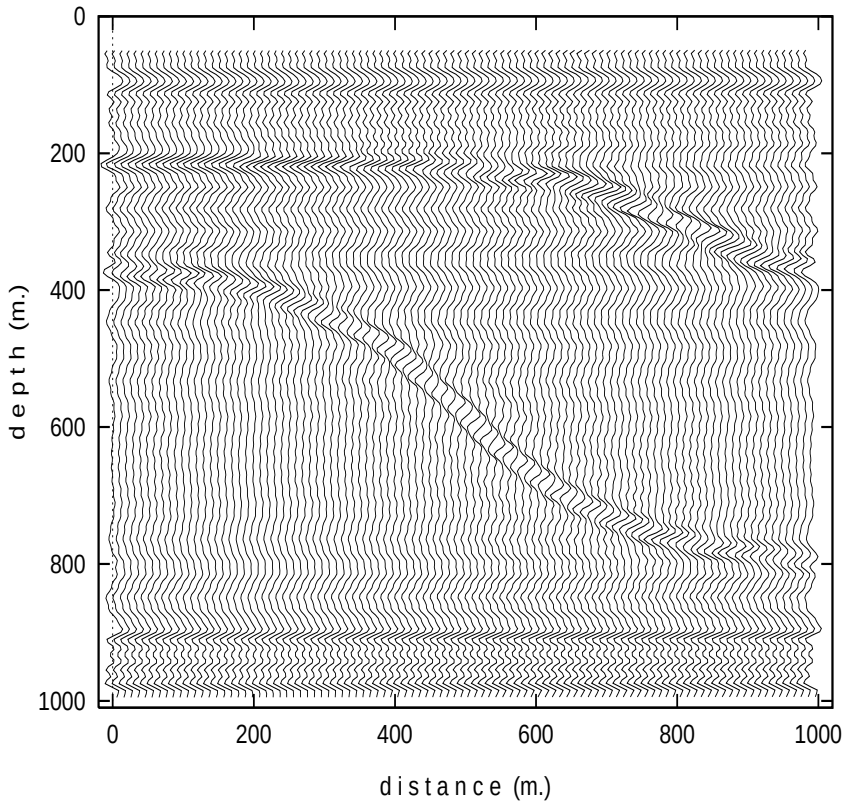

Figure 10: Projection for homogeneous background: a) $\mu \leq 1.5$; b) $\mu \leq 3.5$

a)

b)

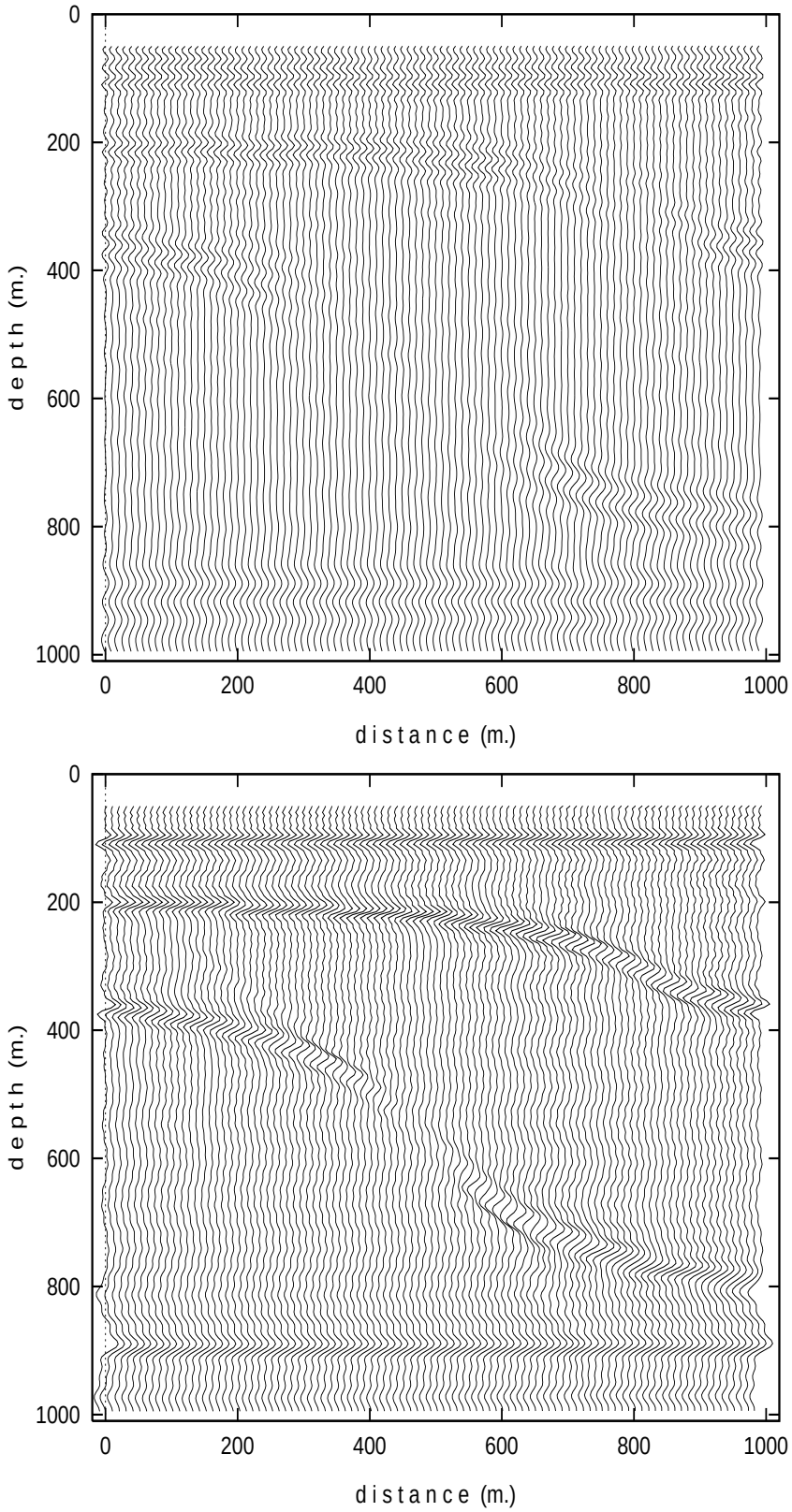

Figure 11: Projection for linear ramp: a) $\mu \leq 4$; b) $\mu \leq 35$

for the second approach it is a subspace of propagators. The truncated SVD allows to control the condition number of a system of equations and, therefore, to regularize the problem. In Tab.1 total dimensions of SVD significant subspaces are given in the last row. A glance to the table is enough to conclude that significant dimension of the problem is very small comparatively with its full dimension.

l	rank		l	rank	
	homogeneous medium	linear ramp		homogeneous medium	linear ramp
1	35	35	2	35	33
3	35	31	4	36	30
5	36	28	6	36	27
7	36	26	8	36	25
9	34	24	10	34	22
11	32	22	12	32	20
13	30	18	14	28	16
15	26	14	16	28	12
17	25	10	18	24	8
19	22	6	20	18	4
21	16	2	22	14	2
23	12	0	24	6	0
25	4	0	26	4	0
27	2	0	28	0	0
29	0	0	30	0	0
			Total:	676	415

Table 1: Values of ranks of matrices A_l for $\mu \leq 1.5$ (homogeneous medium) and $\mu \leq 3.5$ (linear ramp) (for $l \geq 30$ all ranks are equal to zero)

As far as for the propagator/reflectivity decomposition is concerned, dimension of reflectivity subspace is evaluated as $192 \times 192 - (3 \cdot 2^{M_0} \times 3 \cdot 2^{M_0})$ (see section 2). It varies from 36855 for $M_0 = 0$ to 27648 for $M_0 = 5$ and, in particular, for $M_0 = 3$ it is equal to 36288. Hence, one can conclude that the space of reflectivities must have nonempty intersection with the subspace of the smallest singular vectors. Each vector from this intersection belongs to the span of smallest right singular vectors. Image of such a vector under an action of Frechet derivative DB (see sect. 3) is small as $(DB)^*DB$ and $\mathcal{A}^*\mathcal{A}$ are expected to be close one to each other (see Remark 1). As a consequence there should be "invisible" reflectivity (e.g. very thin layers). Another consequence is that after projection onto reflectivity subspace the problem (10) is still ill-posed and in order to get its stable numerical solution some regularization procedure is needed. For example in the MBTT formulation ([1]) the reflectivity is automatically within the orthogonal complement of the forward linearized map, so that it is necessarily a minimum norm solution.

The hypothesis about "almost" orthogonality of subspaces $\mathcal{N}^{(\mu)}$ and subspace of propagators for rather small values of condition number μ (see relation (11) and Remark 2 in Section 4) was checked numerically by computing angles $\alpha_{M_0}^{(\mu)}$ between vectors from $\mathcal{N}^{(\mu)}$ and their orthogonal projection onto subspace of propagators for $M_0 = 2$ and $M_0 = 3$ (see Section 2). More exactly for Synclay model slowness $n(x, z)$ were computed angles between $P_s^{(M_0)}P^{(\mu)}n$ and $P^{(\mu)}n$ ($P_s^{(M_0)}$ is the orthogonal projector onto subspace of propagators). Subspaces $\mathcal{N}^{(\mu)}$ were taken for homogeneous and linear ramp background as described in Section 4. The results are presented in Tab.2. As one can see from the table these subspaces are really "almost" orthogonal for rather small values of condition number μ, while for $\mu = 25$ they are far away from to be orthogonal. We would like to draw the reader attention to the fact that angle $\alpha_{M_0}^{(\mu)}$ decreases under increasing of μ . So, in order to reconstruct a "propagator" component of a slowness one has to deal with $\mathcal{N}^{(\mu)}$ for rather large values of condition number μ, that is with improperly stipulated system of linear algebraic equation (12).

In order to conclude, we would like to draw the attention of the reader to the fact that there is a good coincidence of reflectivity distribution (see Fig.2 and Fig.3) with projections of Synclay model onto subspaces $U^{(\mu)}$ for rather small values of parameter μ.

Subspace $\mathcal{N}^{(\mu)}$	μ	$\|P^{(\mu)}n\|$	$\|P_s^{(2)}P^{(\mu)}n\|$	$\alpha_2^{(\mu)}$	$\|P_s^{(3)}P^{(\mu)}n\|$	$\alpha_3^{(\mu)}$
homogeneous	1.5	$2.13{\cdot}10^{-3}$	$8.81{\cdot}10^{-5}$	88^o	$1.88{\cdot}10^{-4}$	85^o
homogeneous	3.5	$4.10{\cdot}10^{-3}$	$2.80{\cdot}10^{-4}$	86^o	$1.45{\cdot}10^{-3}$	70^o
linear ramp	2.5	$1.35{\cdot}10^{-3}$	$2.53{\cdot}10^{-4}$	80^o	$4.16{\cdot}10^{-4}$	72^o
linear ramp	25	$3.50{\cdot}10^{-3}$	$1.68{\cdot}10^{-3}$	63^o	$2.70{\cdot}10^{-3}$	40^o

Table 2: Angles $\alpha_{M_0}^{(\mu)}$ between vectors from $\mathcal{N}^{(\mu)}$ and their orthogonal projection onto subspace of propagators for $M_0 = 2$ and $M_0 = 3$.

References

[1] G. Chavent and F. Clement. Quantitative migration and resimulation technique for waveform inversion via Migration-Based TravelTime formulation. *Geophysics*, submitted.

[2] G. Chavent and F. Clement. Separating propagation and reflection parameters in the acoustic wave equation. *Geophysics*, submitted.

[3] A. Bamberger, G. Chavent, and P. Lailly. About the stability of the inverse problem in a 1-D wave equation—application to the interpretation of seismic profiles. *Journal of Applied Mathematics and Optimization*, 5:1-47, 1979.

[4] A. Tarantola and B. Valette. Generalized non-linear inverse problems solved using the least-squares criterion. *Review of Geophysics and Space Physics*, 20:219-312, 1982.

[5] F. Jurado, M. Cuer, and V. Richard. 1-D layered media: Part 2, Layer-based waveform inversion. *Geophysics*, 60(6):1857-1874, 1995.

[6] R. Snieder, M. V. Xie, A. Pica and A. Tarantola. Retrieving both the impedance contrast and background velocity: A global strategy for the seismic reflection problem. *Geophysics*, (54):991-1000, 1989.

[7] G. Chavent, C. A. Jacewitz. Determination of background velocities by multiple migration fitting. *Geophysics*, (60):476-490, 1995.

[8] W. W. Symes, J. J. Carrazone. Velocity inversion by differential semblance optimization. *Geophysics*, (56):654-663, 1991.

[9] W. W. Symes, M. Kern. Inversion of reflection seismograms by differential semblance analysis: algorithm structure and synthetic example. *Geophysical Prospecting*, (42):565-614, 1994.

[10] M. S. Gockenbach, W. W. Symes, and R. A. Tapia. The dual regularization approach to seismic velocity inversion. *Inverse Problems*, (11):501-531, 1995.

[11] C. Bunks, F. Mohamed-Saleck, S. Zaleski, and G. Chavent. Multiscale seismic waveform inversion. *Geophysics*, (60):1457-1473, 1995.

[12] L. V. Kantorovich, G. P. Akilov. *Functional Analysis in Normed Spaces*, Pergamon Press, Oxford, England.

[13] W. Symes. On the Relation Between Coefficients and Boundary Values for Solution of Webster's Horn Equation. *SIAM J. Math. Anal.*, (17):1400-1420, 1986.

[14] W. W. Symes. Layered Velocity Inversion: a Model Problem from Reflection Seismology. *SIAM J. Math. Anal.*, (22):680-716, 1991.

[15] W. W. Symes. A Trace Theorem for Solutions of the Wave Equation, and the Remote Determination of Acoustic Sources. v.5, *Math. Meth. in the Appl. Sci.*,(5):131-152, 1983.

[16] W. W. Symes. Some Aspects of Inverse Problems in Several Dimensional Wave Propagation.*Proc. Conference on Inverse Problems, SIAM-AMS Proceedings, ed. D. W. McLaughlin, Amer. Math. Soc., Providence, R.I.*, v.14, 1984.

[17] P. Sacks and W. W. Symes. Uniqueness and Continuous Dependence for a Multidimensional Hyperbolic Inverse Problem. *Comm. in P.D.E.*, (10):635-676, 1985.

[18] Rakesh. A Linearized Inverse Problem for the Wave Equation. *Comm. in P.D.E.*, (13):573-601, 1988.

[19] Z. Sun. On the Uniqueness of a Multidimensional Hyperbolic Inverse Problem. *Comm. in P.D.E.*, (13):1189-1208, 1988.

[20] L. Hörmander. *The Analysis of Linear Partial Differential Operators II: Differential Operators with Constant Coefficients*. Springer-Verlag, Berlin Heidelberg New York Tokyo, 1983.

[21] B. M. Levitan, I. S. Sargsyan. *Introduction to the Spectral Theory* Nauka, Moskva, 1970 (in Russian).

[22] R. H. Stolt. Migration by Fourier transformation. *Geophysics*, (43):23-48, 1978.

[23] P. Lailly. The seismic inverse problem as a sequence of before stack migration. *SIAM Conf. Proc. on Inverse Scattering: Theory and Applications, Eds. J. B. Bednar, E. Robinson, A. Weglein*, 206-220, 1984.

[24] V. I. Kostin, V. A. Tcheverda. r-pseudoinverse for compact operators in Hilbert spaces: existence and stability, *J. of Ill-Posed and Inverse Problems*. (2): 23-46, 1995.

[25] V. I. Kostin, V. G. Khajdukov, V. A. Tcheverda. On r-solution of non-linear equations. in Advanced Mathematics: Computations and Applications, eds. A. S. Alekseev, N. S. Bakhvalov, NCC publisher, 286–291, 1995.

[26] V. G. Khajdukov, V. I. Kostin, V. A. Tcheverda. The r-solution and its applications in linearized waveform inversion for a layered background. *IMA Volume "Inverse Problems of Wave Propagation"*, to appear.

Unité de recherche INRIA Lorraine, Technopôle de Nancy-Brabois, Campus scientifique,
615 rue du Jardin Botanique, BP 101, 54600 VILLERS LÈS NANCY
Unité de recherche INRIA Rennes, Irisa, Campus universitaire de Beaulieu, 35042 RENNES Cedex
Unité de recherche INRIA Rhône-Alpes, 46 avenue Félix Viallet, 38031 GRENOBLE Cedex 1
Unité de recherche INRIA Rocquencourt, Domaine de Voluceau, Rocquencourt, BP 105, 78153 LE CHESNAY Cedex
Unité de recherche INRIA Sophia-Antipolis, 2004 route des Lucioles, BP 93, 06902 SOPHIA-ANTIPOLIS Cedex

Éditeur
INRIA, Domaine de Voluceau, Rocquencourt, BP 105, 78153 LE CHESNAY Cedex (France)
ISSN 0249-6399